universe

IMPACT FACTOR 2.813

CITESCORE 3.2

Article

The Theoretical Description of the Transverse Momentum Spectra: A Unified Model

Rohit Gupta, Anjaly Menon, Shubhangi Jain and Satyajit Jena

Special Issue

Collectivity in High-Energy Proton-Proton and Heavy-Ion Collisions

Edited by

Prof. Dr. Khusniddin Olimov, Prof. Dr. Fu-Hu Liu and Prof. Dr. Kosim Olimov

MDPI

https://doi.org/10.3390/universe9020111

universe

MDPI

Article

The Theoretical Description of the Transverse Momentum Spectra: A Unified Model

Rohit Gupta [1,2], Anjaly Menon [3], Shubhangi Jain [1] and Satyajit Jena [1,*]

[1] Department of Physical Sciences, Indian Institute of Science Education and Research (IISER) Mohali, Sector 81, SAS Nagar, Manauli 140306, Punjab, India
[2] Shaheed Mangal Pandey Government Girls Degree College (SMPGGDC), Jananayak Chandrasekhar University (JNCU), Ballia 277001, Uttar Pradesh, India
[3] Department of Physics, University of Houston, 3507 Cullen Blvd, Houston, TX 77204, USA
* Correspondence: sjena@iisermohali.ac.in

Abstract: Analysis of transverse momentum distributions is a useful tool to understand the dynamics of relativistic particles produced in high-energy collisions. Finding a proper distribution function to approximate the spectra is a vastly developing area of research in particle physics. In this work, we have provided a detailed theoretical description of the unified statistical framework in high-energy physics. We have tested the applicability of this framework on experimental data by analyzing the transverse momentum spectra of pion produced in heavy-ion collision at RHIC and LHC. We have also attempted to explain the transverse momentum spectra of charged hadrons formed in pp collision at different energies using the unified statistical framework. This formalism has been proved to nicely explain the spectra of particles produced in soft processes as well as hard scattering processes in a consistent manner.

Keywords: non-extensive statistical (Tsallis) distributions; high-energy proton–proton and heavy-ion collisions; system equilibration and thermalization; statistical thermal model; transverse momentum spectra of particles

Citation: Gupta, R.; Menon, A.; Jain, S.; Jena, S. The Theoretical Description of the Transverse Momentum Spectra: A Unified Model. *Universe* **2023**, *9*, 111. https://doi.org/10.3390/universe9020111

Academic Editors: Khusniddin Olimov, Fu-Hu Liu and Kosim Olimov

Received: 27 January 2023
Revised: 15 February 2023
Accepted: 17 February 2023
Published: 20 February 2023

1. Introduction

The primary motivation behind theoretical and experimental studies in particle physics is to enhance our knowledge about the fundamental constituents of matter that make up the universe. One integral component that is elemental in our understanding of the matter content of the universe is the state called Quark-Gluon Plasma (QGP) which was created a few microseconds after the Big Bang. Theoretical calculations based on Lattice Quantum Chromodynamics (LQCD) framework first predicted the existence of this new state at sufficiently high temperatures or baryon densities, which were present at the very early stage of Universe expansion. Later, heavy-ion collision experiments performed at Relativistic Heavy Ion Collider (RHIC) [1] and Large Hadron Collider (LHC) [2] made it possible to reach energy densities above critical values predicted by Lattice QCD, for the formation of QGP [3–5]. Since the QGP droplet is being created for an extremely short interval of time (10^{-22} s) so it is not possible, with present technologies, to directly probe this state. Hence we rely on the kinematics observables such as rapidity, transverse momenta, and energy of the final state particles to extract information of such initial state. One such kinematics observable is the transverse momentum p_{T}-spectra, which is the component of momentum in the direction transverse to the beam direction.

In this paper, we focus on studying transverse momentum distributions, which have proven to be a useful probe for understanding the thermodynamic properties and the evolutionary dynamics of systems produced in relativistic heavy-ion collisions. Our objective is to find a proper distribution function that approximates and explains the transverse momentum spectra. We begin with a short review of developments that happened on this

path of finding a distribution that can explain particle spectra with better accuracy. Later a solution to the problem is proposed using Pearson distribution [6].

In Section 2, we discuss different statistical frameworks that have been used for understanding thermal QGP systems, including Boltzmann (BG) and Tsallis frameworks. These two models are chosen since these are the most fundamental statistical thermal models; however, a comparison with other models, including flow effect, etc. is provided in Ref. [7]. We introduce our proposal to the problem using a generalized distribution called Pearson distribution. A detailed formulation of the generalized function is performed, allowing us to write the unified function as an extended form of Tsallis distribution. The validation, goodness of the fit parameter, and analyses are given in Section 3. Finally, we conclude with a discussion in Section 4.

2. Statistical Approach to Thermal Qgp Systems

Transverse momentum spectra play a pivotal role in enhancing our knowledge of the thermal and bulk properties of QCD matter produced during the heavy-ion collision. However, to extract the parameter of interest, the theoretical model is required to explain the spectra consistently. Although QCD is the underlying theory to explain such a strongly interacting system, it is a challenging task to apply QCD to explain the spectra in a low-p_{T} regime due to the asymptotic freedom at the perturbative order where the coupling strength is very high. Hence, we resort to a statistical thermal approach to explain the spectra.

A proposal to apply statistical models to explain particle production was given for the first time in 1948 by Koppe [8,9]. Two years later, Fermi introduced a statistical framework [10,11] to study the energy distribution of particles coming out from the small volume where a large amount of energy is concentrated when two nucleons with a high center of mass energy collide with each other. Although the Fermi model was a reliable description of energy ranges comparable to that of cosmic rays, it breaks down at lower energies. The first systematic description of the mass spectrum of strongly interacting particles based on the asymptotic bootstrap principle was formulated by Hagedorn [12,13] in 1965. The Hagedorn model introduces a limiting temperature T_0, which is the highest possible temperature for the strong interaction. Using this model, it was possible to accurately determine the total multiplicity of hadronic particles produced in collisions.Even now, its modified version is used to understand the hadronic phase in high-energy collisions. These works on the statistical description of particle spectra in high-energy physics are followed by many papers over the past several decades on the characterization of particle production using statistical mechanics. A detailed review of the application of statistical thermal models can be found in Ref. [14].

In standard thermodynamics, we characterize a macroscopic system using state variables like number density (n), energy density (ϵ), pressure (p), temperature (T), and chemical potential (μ). The equilibrium thermodynamic properties of hadronic systems obtained using statistical models can also be characterized by the thermodynamic parameters mentioned above. This will finally give insights into the dynamics of the systems in terms of these state variables. Certain aspects of the relativistic kinetic theory are also used in this statistical description. Considering a system of a large number of relativistic particles, all the macroscopic quantities required for the thermodynamic description of the system can be derived by using the partition function, which describes the distribution of particles in a thermodynamics system in equilibrium. The definitions of parameters like energy density, pressure, and momentum, in terms of the partition function, can be found in Ref. [15]. In the next few subsections, we present the BG and Tsallis statistical framework, which have been used to understand the system of relativistic particles.

2.1. Boltzmann–Gibbs Statistics

Considering the system produced in high energy collision to be of thermal origin, the most natural choice to describe the distribution of particles will be Maxwell-

Boltzmann statistics [16,17]. Since the temperature of the system produced in a collision is extremely high and Fermi–Dirac and Bose–Einstein statistical system tends toward Maxwell–Boltzmann statistics at high temperatures, it will be justifiable to use Boltzmann statistics to explain the particle production spectra in the collision.

In general, the expression for the average number of particles in the sth state of a statistical system is given as:

$$n_s = \frac{1}{e^{\beta(\epsilon_s-\mu)} \pm 1} \tag{1}$$

If the number of particles in the system is constant, the constraint determining μ will be given in terms of the following equation.

$$\sum_s n_s = \frac{1}{e^{\beta(\epsilon_s-\mu)} \pm 1} = N \tag{2}$$

where the upper and lower sign refers to the case of Bosons and Fermions, respectively. When we look at the classical limit, which is defined by high temperature, the higher energy states will be mostly occupied and the relation $\epsilon_s >> \mu$ will be obeyed.

For keeping N fixed, the $e^{\beta\epsilon_s-\mu} >> 1$ relation must be satisfied. When this is satisfied, the functional form for the number of particles will become exponential like or BG distribution as follows:

$$n_s = e^{-\beta(\epsilon_s-\mu)} \tag{3}$$

From the standard statistical thermodynamics, we know that the probability of each microstate or the population of particles to occupy each state in a thermal system at equilibrium is an exponential function of energy. For a system of particles following Boltzmann distribution, the number density will be given as

$$n' = \frac{g}{(2\pi)^3} \int d^3p \; exp\left(\frac{\mu - E}{T}\right) \tag{4}$$

which can be written in differential form as

$$\frac{d^3N}{dp^3} = \frac{gV}{(2\pi)^3} \; exp\left(\frac{\mu - E}{T}\right) \tag{5}$$

Here, g is the spin degeneracy factor and is equal to 1 for pseudoscalar mesons (pions, kaons) and 2 for spin half particles (proton and anti-proton). Expanding the momentum variable in three dimensions in polar coordinates will give

$$d^3p = 2\pi p_T \; dp_T dp_z$$

where p_T and p_z are transverse and longitudinal momentum, respectively. Therefore, upon equating right hand side of the Equation (5) we will get

$$E\frac{d^3N}{dp^3} = \frac{d^2N}{dp_T^2 dy} = \frac{d^2N}{2\pi p_T dp_T dy} \tag{6}$$

Here we used the relation $\frac{dp_z}{E} = dy$ where y is the rapidity variable. Using this we will modify Equation (5) to the form

$$\frac{d^2N}{2\pi p_T dp_T dy} = E\frac{gV}{(2\pi)^3} \; exp\left(\frac{\mu - E}{T}\right) \tag{7}$$

We can replace E by $m_T cosh y$ where $m_T = \sqrt{m^2 + p_T^2}$ is transverse mass. Further, using the fact that at LHC energies μ is vanishing because of approximately equal production of particle and anti-particles and in mid-rapidity region $cosh y \simeq 1$ $(y = 0)$, we can get

$$\frac{d^2N}{2\pi p_T dp_T dy} = m_T \frac{gV}{(2\pi)^3} exp\left(\frac{-m_T}{T}\right) \tag{8}$$

The above expression has been used extensively to fit the transverse momentum spectra of different particles produced in the collision [17–19].

Although this formalism finds its application in many different fields, including high-energy physics, there are several issues in explaining the data that need to be addressed. The application of Maxwell–Boltzmann distribution is limited to the sample where the number of constituents in a system is of the order of Avogadro number $(N_A = 6.023 \times 10^{23})$. However, in heavy-ion collision, only a few thousand particles are getting produced, limiting the applicability of BG statistics to the collision data sample. This difference is also reflected in the deviation of experimental data from the BG function, which fits the experimental data only in a narrow range of p_{T} and deviates significantly at low as well as high p_{T}. Further, BG distribution only applies to the system where entropy is additive and extensive. However, many physical systems involve long-range interactions and phase space of complex microscopic dynamics that violate BG statistical mechanics and standard thermodynamics. Hence a generalization of BG distribution was required to include the non-extensive system. Tsallis [20] put forward this generalization in 1988, and since then, it has been extensively used to study the thermodynamical properties of particles produced in high energy collisions.

2.2. Tsallis Statistics

The generalization of the Boltzmann–Gibbs theory, known as non-extensive statistical mechanics, was initially constructed based on an entropy proposed by Tsallis in 1988. This entropy, called Tsallis entropy, has a form that converges to that of BG entropy in a specific limit of its q-parameter. The 'q' works as a scaling factor to make standard statistical mechanics applied to the systems where the number of constituents is considerably lower than the Avogadro number. Thus, this parameter in the Tsallis distribution gives the extent of non-extensivity in the thermodynamical system.

Since the Tsallis statistics has an intrinsic scaling factor in its construction, it is extensively used to explain systems where temperature fluctuations are present around some initial value T_0. In such cases, the q parameter, which tells about non-extensivity in the system, can be connected to the variance of temperature [21,22] as

$$q - 1 = \frac{Var(T)}{\langle T \rangle^2} \tag{9}$$

One major modification in the algebra related to Tsallis statistics is the introduction of q-exponential and q-logarithm given as

$$exp_q(x) = [1 - (q-1)x]^{-\frac{1}{q-1}} \tag{10}$$

and

$$ln_q(p_i) = \begin{cases} ln(p_i), & \text{if } p_i \geq 0, q = 1 \\ \frac{p_i^{1-q} - 1}{1-q}, & \text{if } p_i \geq 0, q \neq 1 \\ undefined, & \text{if } p_i \leq 0 \end{cases}$$

Non-extensive entropy as proposed by Tsallis [20] is defined as

$$S_q = -k\sum_i p_i^q ln_q(p_i) \tag{11}$$

$$= -k\sum_i p_i^q \frac{p_i^{1-q}-1}{1-q} \tag{12}$$

$$= -k\sum_i \frac{p_i - p_i^q}{1-q} \tag{13}$$

$$= k\frac{1-\sum_i p_i^q}{q-1} \tag{14}$$

which in the limit $q \longrightarrow 1$ gives standard Gibbs entropy

$$S = -k\sum_i p_i ln(p_i) \tag{15}$$

As we discussed earlier, the BG approximation to transverse momentum spectra fails at lower and higher momentum ranges.In contrast, the Tsallis approximation works better, and numerous studies have been performed using the same motivation of Tsallis statistics to particle production spectra [21,23,24]. The thermodynamical aspects of this formalism and its foundations and applications are discussed in [25,26]. In this context, we can easily obtain Tsallis statistical distribution used for fitting transverse momentum data from BG distribution by replacing the exponential in BG function with q-exponential. In addition, the distribution function used for fitting to particle spectra can be derived accordingly where m_T, p_T, T, g, and V have the same meaning as in BG distribution and y is the rapidity variable.

$$\frac{1}{2\pi p_T}\frac{d^2N}{dp_T dy} = \frac{gVm_T}{(2\pi)^3}\left[1+(q-1)\frac{m_T-\mu}{T}\right]^{-\frac{q}{q-1}} \tag{16}$$

The definition of Tsallis's statistical version of Fermi–Dirac and Bose–Einstein distributions and corresponding entropy functionals are given in [23]. As we can define the number density, energy density, pressure, etc. in BG formalism [15], similar can be done using non-extensive relativistic kinetic theory. The only difference is that the Tsallis distribution function will be raised to power q. In standard thermodynamics, we are familiar with the constraints on the total number of particles, N, and energy, E, in the system. Given the distribution function f_i,

$$N = \sum_i f_i \tag{17}$$

$$E = \sum_i f_i E_i \tag{18}$$

whereas in Tsallis's case, the above constraints must be redefined in the following way with the function raised to a power of q.

$$\begin{aligned} N &= \sum_i f_i^q \\ E &= \sum_i f_i^q E_i \end{aligned} \tag{19}$$

The appropriate definition of entropy to accommodate positive entropy production according to the second law of thermodynamics is given in [27]. Further, in the classical limit, Tsallis entropy will have the following functional form as explained in [23].

$$S_T = -g\sum_i (f_i^q ln_q f_i - f_i) \tag{20}$$

Here, $ln_q(x)$ is the q-logarithm and is defined as

$$ln_q(x) \equiv \frac{x^{1-q}-1}{1-q} \tag{21}$$

Therefore, by expanding the form of entropy, we will get

$$S_T = g\sum_i \left[\frac{qf_i}{q-1} - \frac{f_i^q}{q-1}\right] \tag{22}$$

By maximizing the above entropy under the constraints given in Equation (19) we will get a variational equation:

$$\frac{\delta}{\delta f_i}\left[S_T + \alpha\left(N - \sum_i f_i^q\right) + \beta\left(E - \sum_i f_i^q E_i\right)\right] = 0 \tag{23}$$

Here α and β are the Lagrange multipliers for the total number of particles and total energy, respectively. Solving this equation, we will get distribution function (f_i).

$$f_i = \left[1 + (q-1)\frac{E_i - \mu}{T}\right]^{-\frac{1}{q-1}} \tag{24}$$

It can be easily shown that the entropy defined above will give Tsallis distribution function under its extremization. However, this distribution function must be thermodynamically consistent, which can be shown by checking whether the relations among thermodynamic parameters are indeed obeyed. In Ref. [23], the Tsallis function has been proved to be consistent with respect to the laws of standard thermodynamics.

2.3. Hard Processes and Limitation in Tsallis Statistics

Tsallis statistics has been used extensively to describe high energy systems, particularly for describing transverse momentum spectra. In Ref. [23], after proving the thermodynamic consistency of the Tsallis distribution function, a modified form is proposed, and the fit details are also presented. In another work [21,24], a review on implementing non-extensive statistical mechanics for the description of heavy-ion collisions is given, together with new interpretations for the non-extensivity parameter q. In [28,29], different power laws used in explaining high-energy processes and the importance of non-extensive formalism are discussed. Another work from literature is [30], where p_{T}-spectra of negatively charged pions are fitted with a standard function and its Tsallis form, and a comparison is made. The non-extensive Tsallis approach provides better fits and explains heavy-ion collisions more appropriately as compared to the standard Boltzmann and power-law approaches. The plots of p_{T}-spectra of π^+ and π^- particles fitted to Tsallis function is displayed in [31], where satisfying agreement between the experimental data and function is established. However, it is known that the exponential function or standard BG theory can only take care of the soft p_{T} region of the hadronic spectra where the particles produced will have small transverse momenta. Whereas QCD calculations have shown that power-law functions can explain spectra of particles produced in hard scattering processes [30,32].

For the low-p_{T} part of the spectra (corresponding to the "soft sector"), the methods described above and their variants have been used extensively to study the spectra. However, particle production in a high p_{T} regime is dominated by hard QCD scattering processes, and corresponding spectra follow a power law. It is difficult to explain these two regions of the spectra using a single probability distribution function. Hence, several two-component models have been devised to explain the full range of the spectra. However, it is difficult to determine the clear boundary between the two regions of the spectra [33]. Notably, we intend to find a master distribution function that describes the whole region of p_{T}-spectra (both soft and hard parts) in a unified manner.

Although the Tsallis approach takes care of the generalization upto some extent [31], it has been shown in a recent paper [30,33] that the Tsallis distribution, in its purest form, can describe only the low-p_T range of the spectra, which belongs to the particles produced in soft excitation process. In Ref. [34,35], compatibility of Tsallis statistics with p_T-spectra at large transverse momenta has been established in pp collision; however, apparent deviation from the data is observed in the higher momentum range of the spectra of particles produced in the heavy-ion collision as can be seen in the figures. Some efforts are being made to modify Tsallis statistics to explain the hard part of the spectra [36,37]; however, the search for a consistent framework to explain the spectra is still an open question.

Since perturbative QCD can be used to describe hard scattering processes, it is possible to extract the form of p_T-spectra at these regions. In addition, the calculations suggest that the spectra will have the form of inverse power law, which is expressed as [30,32,38–41]:

$$f(p_T) = \frac{1}{N}\frac{dN}{dp_T} = Ap_T\left(1+\frac{p_T}{p_0}\right)^{-n} \tag{25}$$

where p_0 and n are fitting parameters and A is the normalization constant related to free parameters. This QCD-inspired model was proposed by Hagedorn [42] to describe the data of an invariant cross-section of hadrons as a function of p_T. Our proposal to the question above stated is to combine inverse power-law and Tsallis distribution using Pearson distribution. This statistical approach is discussed in detail in the following sections.

2.4. A Generalization of Tsallis Statistics

A comprehensive approach is to look into the parent equation of the Tsallis family of equations, which must have more parameters yet controllable mechanisms to hold thermodynamics laws. Following the same argument, we look upon the Pearson distribution, which intrinsically deals with more parameters and is controlled by the first four fours moments of the distribution, making a perfect choice for our case. The proposal for Pearson distribution was first given by Karl Pearson in 1895 [43] and subsequently modified in 1901 and 1916. His main idea was to categorize any distribution function based on the first four moments related to the mean, standard deviation, skewness, and kurtosis of the distribution. Moments are defined for specifying the shape of any probability distribution. The first moment or the mean locates at the center of the distribution, whereas variance gives the spread or dispersion in the data about the mean. The other two are called shape parameters, among which skewness provides the degree of asymmetry in the distribution around the mean and kurtosis specifies the relative peakedness or flatness of the distribution. Characterization of any statistical data involves the specification of skewness and kurtosis.

Gaussian, Beta, Gamma, inverse-gamma, exponential, and Student's T-distribution are all special cases in the Pearson distribution and belong to the Pearson family of curves. Thus, it is considered the most general distribution and has been used in many different fields like geophysics, bio-statistics, and financial marketing. It is a family of continuous probability distributions whose densities $p(x)$ satisfy the following differential equation [44].

$$\frac{1}{p(x)}\frac{dp(x)}{dx} + \frac{a+x}{b_0+b_1x+b_2x^2} = 0 \tag{26}$$

where the parameters a, b_0, b_1, b_2 can be related to the first four central moments as follows:

$$a = b_1 = \frac{m_3(m_4+3m_2^2)}{10m_2m_4-18m_2^3-12m_3^2} \tag{27}$$

$$b_0 = \frac{m_2(4m_2m_4-3m_3^2)}{10m_2m_4-18m_2^3-12m_3^2} \tag{28}$$

$$b_2 = \frac{2m_2m_4 - 6m_2^3 - 3m_3^2}{10m_2m_4 - 18m_2^3 - 12m_3^2} \tag{29}$$

Here, m_1, m_2, m_3, and m_4 are the first four central moments with $m_1 = 0$. Pearson curves are classified into 12 different types based on the root of the quadratic equation in the denominator of the differential equation. Therefore, Pearson criteria which will decide the type of distribution is the sign of discriminant of the quadratic equation, which is expressed as,

$$k = \frac{b_1^2}{4b_0b_2} \tag{30}$$

A table including different types of Pearson distribution along with Pearson criteria and conditions on parameters can be found in Refs. [45,46]. Further, solving the differential Equation (26), we can find the Pearson density as follows:

$$p(x) = C' \exp \int -\frac{P(x)}{Q(x)}dx \tag{31}$$

$$= C' \exp \int -\frac{a_0 + a_1x}{b_0 + b_1x + b_2x^2}dx \tag{32}$$

We can express the quadratic equation in the following form,

$$b_0 + b_1x + b_2x^2 = b_2(x + \alpha)(x + \beta) \tag{33}$$

$$p(x) = \frac{C'}{-b_2} \exp \int \frac{a_0 + a_1x}{(x + \alpha)(x + \beta)}dx \tag{34}$$

$$= C \exp \int \left(\frac{v}{x + \alpha} + \frac{w}{x + \beta} \right) dx \tag{35}$$

where v and w have following definition:

$$v = -\frac{a_0 - a_1\alpha}{\alpha - \beta} \qquad w = \frac{a_0 - a_1\beta}{\alpha - \beta} \tag{36}$$

After integration,

$$p(x) = C \exp\{ln(x + \alpha)^v + ln(x + \beta)^w\} \tag{37}$$

$$= C(x + \alpha)^v(x + \beta)^w \tag{38}$$

A general solution can be written as in Equation (39) where C is a normalization constant and e, f, g, and h are free parameters.

$$p(x) = C(e + x)^f(g + x)^h \tag{39}$$

Pearson's family of distributions give an advantage of extra free parameter yet preserving all previous models. At this stage, going back to our initial argument, we can show how the Pearson equation is reducible to Tsallis in the limiting case. The Pearson function can be expressed as an extended version of the Tsallis distribution. It is easy to see that the Pearson distribution converges to exponential when the numerator, $P(x)$, and denominator, $Q(x)$ in Equation (31) becomes constant and unity, respectively. Similarly, we can derive the limit of Pearson parameters at which it will reduce to Normal or Gaussian distribution. For this, $P(x)$ has to be of a linear form, and $Q(x)$ has to be unity. Since Pearson density reduces to exponential at some limit, it is possible to find a relation between Tsallis, which

is a generalized Boltzmann, and the Pearson function. The Equation (39) can be rewritten in the following form by doing simple algebra.

$$p(x) = B\left(1+\frac{x}{e}\right)^{f}\left(1+\frac{x}{g}\right)^{h} \tag{40}$$

Up to some normalization constant $B = Ce^f g^h$. Now if we replace $g = \frac{T}{q-1}$, $h = -\frac{q}{q-1}$, $f = -n$ and $e = p_0$ we will get:

$$p(x) = B\left(1+\frac{p_T}{p_0}\right)^{-n}\left(1+(q-1)\frac{p_T}{T}\right)^{-\frac{q}{q-1}} \tag{41}$$

where,

$$B = C\frac{1}{(p_0)^n}\left(\frac{T}{q-1}\right)^{-\frac{q}{q-1}} \tag{42}$$

This makes it a perfect choice to fit the particle spectra with this function.

$$\frac{1}{2\pi p_T}\frac{d^2N}{dp_T dy} = B'\left(1+\frac{p_T}{p_0}\right)^{-n}\left(1+(q-1)\frac{p_T}{T}\right)^{-\frac{q}{q-1}} \tag{43}$$

where $B' = B \times \frac{V}{(2\pi)^3}$ with the additional $\frac{V}{(2\pi)^3}$ comes when we move from summation to integration. Hence, it is inferred that the unified distribution is a generalized form of the Tsallis distribution and can be shown to have two parts. In reference to Equation (25), the inverse power law term in the above equation can be considered as the hard scattering part in the extended Tsallis form of distribution.

At the same time, the backward compatibility of the distribution makes it a more prominent and stable equation to be considered while proposing a generalization. In the context of unified distribution, since it is proposed to be a generalization of Tsallis hence, it should reduce to Tsallis distribution under some limit on parameters. We observed that the unified distribution (43) is backward compatibility in the limit $n = -1$ and $p_0 = 0$. This means that in the limitations discussed above, the unified distribution reduces to the Tsallis distribution preserving all thermodynamic properties. Hence, we can describe unified distribution as the generalization of Tsallis distribution with an additional part to explain the higher-p_T part of the spectra corresponding to the particles produced in hard scattering processes.

2.5. Thermodynamical Consistency Check for Unified Distribution

The proposed equation must pass the thermal test, in this context, a procedure similar to that used for the Tsallis framework is followed with a modified form of Tsallis entropy. To show the thermodynamical consistency of the distribution, following relation [23] must be satisfied:

$$T = \left.\frac{\partial \epsilon}{\partial s}\right|_{n} \tag{44}$$

$$\mu = \left.\frac{\partial \epsilon}{\partial n'}\right|_{s} \tag{45}$$

$$n' = \left.\frac{\partial P}{\partial \mu}\right|_{T} \tag{46}$$

$$s = \left.\frac{\partial P}{\partial T}\right|_{\mu} \tag{47}$$

The constraint equation of the total number of particles and total energy remains the same as in the Tsallis distribution:

$$\begin{aligned} N &= \sum_i f_i^q \\ E &= \sum_i f_i^q E_i \end{aligned} \tag{48}$$

In the case of a unified distribution

$$E\frac{d^3N}{dp^3} = B'\left(1+\frac{E}{p_0}\right)^{-n}\left(1+(q-1)\frac{(E-\mu)}{T}\right)^{-\frac{q}{q-1}} \tag{49}$$

$$\frac{d^3N}{dp^3} = \frac{B'}{E}\left(1+\frac{E}{p_0}\right)^{-n}\left(1+(q-1)\frac{(E-\mu)}{T}\right)^{-\frac{q}{q-1}} \tag{50}$$

We can simplify the above equation to

$$\frac{d^3N}{dp^3} = B' f_E f_{Ta}^q \tag{51}$$

where

$$f_E = \frac{1}{E}\left(1+\frac{E}{p_0}\right)^{-n} \tag{52}$$

$$f_{Ta} = \left(1+(q-1)\frac{(E-\mu)}{T}\right)^{\frac{-1}{q-1}} \tag{53}$$

Hence, we have

$$\frac{d^3N}{dp^3} = \frac{V}{(2\pi)^3}\left\{(Bf_E)^{\frac{1}{q}} f_{Ta}\right\}^q \tag{54}$$

or more generally,

$$\frac{d^3N}{dp^3} = \frac{V}{(2\pi)^3} f_i^q \tag{55}$$

where

$$f_i = \left(Bf_{E_i}\right)^{\frac{1}{q}} f_{Ta_i} \tag{56}$$

Entropy in the case of unified distribution is given as

$$S_p = \sum_i \left[\frac{q f_i}{(q-1)\left(Bf_{E_i}\right)^{\frac{1}{q}-1}} - \frac{f_i^q}{q-1}\right] \tag{57}$$

With this form of entropy, we can solve Equation (23) to get the form of distribution function Equation (56).

For consistency check, we have to prove the basic thermodynamic relations given in Equations (44)–(47).

2.5.1. Relation 1

First of the relations above is the derivative of energy density with respect to entropy density given as

$$T = \left.\frac{\partial \epsilon}{\partial s}\right|_{n'} \tag{58}$$

Solving the right-hand part of the equation

$$\left.\frac{\partial E}{\partial S}\right|_{n'} = \frac{\frac{\partial E}{\partial T}dT + \frac{\partial E}{\partial \mu}d\mu}{\frac{\partial S}{\partial T}dT + \frac{\partial S}{\partial \mu}d\mu} \tag{59}$$

$$\left.\frac{\partial E}{\partial S}\right|_{n'} = \frac{\frac{\partial E}{\partial T} + \frac{\partial E}{\partial \mu}\frac{d\mu}{dT}}{\frac{\partial S}{\partial T} + \frac{\partial S}{\partial \mu}\frac{d\mu}{dT}} \tag{60}$$

In this relation, n' is constant, which add an additional constraint

$$dn' = \frac{\partial n'}{\partial T}dT + \frac{\partial n'}{\partial \mu}d\mu = 0 \tag{61}$$

$$\frac{d\mu}{dT} = -\frac{\frac{\partial n'}{\partial T}}{\frac{\partial n'}{\partial \mu}} \tag{62}$$

Solving for components of Equation (60)

$$\frac{\partial E}{\partial T} = \sum_i q f_i^{q-1} E_i \frac{\partial f_i}{\partial T} \tag{63}$$

$$\frac{\partial E}{\partial \mu} = \sum_i q f_i^{q-1} E_i \frac{\partial f_i}{\partial \mu} \tag{64}$$

$$\frac{\partial S}{\partial T} = \sum_i \frac{q}{(q-1)\left(B f_{E_i}\right)^{\frac{1}{q}-1}} \frac{\partial f_i}{\partial T} - \frac{q f_i^{q-1}}{q-1}\frac{\partial f_i}{\partial T} \tag{65}$$

$$\frac{\partial S}{\partial \mu} = \sum_i \frac{q}{(q-1)\left(B f_{E_i}\right)^{\frac{1}{q}-1}} \frac{\partial f_i}{\partial \mu} - \frac{q f_i^{q-1}}{q-1}\frac{\partial f_i}{\partial \mu} \tag{66}$$

$$\frac{\partial n'}{\partial T} = \frac{1}{V}\sum_i q f_i^{q-1}\frac{\partial f_i}{\partial T} \tag{67}$$

$$\frac{\partial n'}{\partial \mu} = \frac{1}{V}\sum_i q f_i^{q-1}\frac{\partial f_i}{\partial \mu} \tag{68}$$

Simplifying the numerator of Equation (60)

$$\frac{\partial E}{\partial T} + \frac{\partial E}{\partial \mu}\frac{d\mu}{dT} = \sum_i q E_i f_i^{q-1}\frac{\partial f_i}{\partial T} - \frac{\sum_{i,j} q^2 E_i (f_i f_j)^{q-1}\frac{\partial f_i}{\partial \mu}\frac{\partial f_j}{\partial T}}{\sum_j q f_j^{q-1}\frac{\partial f_j}{\partial \mu}} \tag{69}$$

This can be further reduced to

$$\frac{\partial E}{\partial T} + \frac{\partial E}{\partial \mu}\frac{d\mu}{dT} = \frac{\sum_{i,j} q E_i (f_i f_j)^{q-1} C_{ij}}{\sum_j f_j^{q-1}\frac{\partial f_j}{\partial \mu}} \tag{70}$$

where

$$C_{ij} = \left\{\frac{\partial f_i}{\partial T}\frac{\partial f_j}{\partial \mu} - \frac{\partial f_i}{\partial \mu}\frac{\partial f_j}{\partial T}\right\} \tag{71}$$

Similarly solving for the denominator part of Equation (60)

$$\frac{\partial S}{\partial T}+\frac{\partial S}{\partial \mu}\frac{d\mu}{dT} = \frac{\sum\limits_{i,j}\left\{\frac{qf_j^{q-1}}{(q-1)(Bf_E)^{\frac{1}{q}-1}}-\frac{q(f_if_j)^{q-1}}{q-1}\right\}C_{ij}}{\sum\limits_j f_j^{q-1}\frac{\partial f_j}{\partial \mu}} \tag{72}$$

From Equations (70) and (72), we get

$$\left.\frac{\partial E}{\partial S}\right|_{n'} = \frac{\sum\limits_{i,j} qE_i(f_if_j)^{q-1}C_{ij}}{\sum\limits_{i,j}\left(\frac{q}{q-1}\right)\left[\frac{f_j^{q-1}}{(Bf_{E_i})^{\frac{1}{q}-1}}-(f_if_j)^{q-1}\right]C_{ij}} \tag{73}$$

$$\left.\frac{\partial E}{\partial S}\right|_{n'} = \frac{T\sum\limits_{i,j} E_i(f_if_j)^{q-1}C_{ij}}{\sum\limits_{i,j}[E_i(f_if_j)^{q-1}C_{ij}-\mu(f_if_j)^{q-1}C_{ij}]} \tag{74}$$

However, $\sum\limits_{i,j} C_{ij} = 0$ and also $(f_if_j)^{q-1} = (f_jf_i)^{q-1}$. So the term with μ in the denominator becomes zero, and hence we get

$$\left.\frac{\partial \epsilon}{\partial s}\right|_{n'} = T \tag{75}$$

which proves that the relation Equation (44) is satisfied for unified distribution.

2.5.2. Relation 2

The second thermodynamic relation is given as

$$\left.\frac{\partial \epsilon}{\partial n'}\right|_{s} = \mu \tag{76}$$

$$\left.\frac{\partial E}{\partial N}\right|_{s} = \frac{\frac{\partial E}{\partial T}dT+\frac{\partial E}{\partial \mu}d\mu}{\frac{\partial N}{\partial T}dT+\frac{\partial N}{\partial \mu}d\mu} \tag{77}$$

$$\left.\frac{\partial E}{\partial N}\right|_{s} = \frac{\frac{\partial E}{\partial T}+\frac{\partial E}{\partial \mu}\frac{d\mu}{dT}}{\frac{\partial N}{\partial T}+\frac{\partial N}{\partial \mu}\frac{d\mu}{dT}} \tag{78}$$

Here s is constant so

$$ds = \frac{\partial s}{\partial T}dT+\frac{\partial s}{\partial \mu}d\mu = 0 \tag{79}$$

$$\frac{d\mu}{dT} = -\frac{\frac{\partial s}{\partial T}}{\frac{\partial s}{\partial \mu}} \tag{80}$$

$$\frac{\partial E}{\partial T}+\frac{\partial E}{\partial \mu}\frac{d\mu}{dT} = \frac{\sum\limits_{i,j}\left(\frac{qE_if_i^{q-1}}{\left(Bf_{E_j}\right)^{\frac{1}{q}-1}}-qE_i(f_if_j)^{q-1}\right)C_{ij}}{\sum\limits_j\left(\frac{1}{\left(Bf_{E_j}\right)^{\frac{1}{q}-1}}\frac{\partial f_j}{\partial \mu}-f_j^{q-1}\frac{\partial f_j}{\partial \mu}\right)} \tag{81}$$

Similarly, for the N part, we get

$$\frac{\partial N}{\partial T} + \frac{\partial N}{\partial \mu}\frac{d\mu}{dT} = \frac{\sum_{i,j}\left(\frac{q f_i^{q-1}}{\left(B f_{E_j}\right)^{\frac{1}{q}-1}} - q(f_i f_j)^{q-1}\right) C_{ij}}{\sum_j\left(\frac{1}{\left(B f_{E_j}\right)^{\frac{1}{q}-1}}\frac{\partial f_j}{\partial \mu} - f_j^{q-1}\frac{\partial f_j}{\partial \mu}\right)} \tag{82}$$

On dividing the above equations, we get

$$\frac{\frac{\partial E}{\partial T} + \frac{\partial E}{\partial \mu}\frac{d\mu}{dT}}{\frac{\partial N}{\partial T} + \frac{\partial N}{\partial \mu}\frac{d\mu}{dT}} = \frac{\sum_{i,j}\left(\frac{q E_i f_i^{q-1}}{\left(B f_{E_j}\right)^{\frac{1}{q}-1}} - q E_i (f_i f_j)^{q-1}\right) C_{ij}}{\sum_{i,j}\left(\frac{q f_i^{q-1}}{\left(B f_{E_j}\right)^{\frac{1}{q}-1}} - q(f_i f_j)^{q-1}\right) C_{ij}} \tag{83}$$

The equation above reduces to

$$\left.\frac{\partial \epsilon}{\partial n'}\right|_s = \mu \tag{84}$$

2.5.3. Relation 3

Now consider the third relation:

$$\left.\frac{\partial P}{\partial \mu}\right|_T = n' \tag{85}$$

where n' is the number density. From laws of thermodynamics, we get

$$P = \frac{-E + TS + \mu N}{V} \tag{86}$$

$$\left.\frac{\partial P}{\partial \mu}\right|_T = \frac{1}{V}\left[\frac{-\partial E}{\partial \mu} + T\frac{\partial S}{\partial \mu} + N + \mu\frac{\partial N}{\partial \mu}\right] \tag{87}$$

$$\left.\frac{\partial P}{\partial \mu}\right|_T = \frac{1}{V}\sum_i\left[f_i^q - \frac{T}{q-1}\left\{1 + (q-1)\frac{(E_i - \mu)}{T}\right\}\frac{\partial f_i^q}{\partial \mu} + \frac{Tq}{q-1}\frac{1}{\left(B f_{E_i}\right)^{\frac{1}{q}-1}}\frac{\partial f_i}{\partial \mu}\right] \tag{88}$$

$$f_i = \left(B f_{E_i}\right)^{\frac{1}{q}} f_{Ta_i} \tag{89}$$

$$\frac{\partial f_i}{\partial \mu} = \frac{\left(B f_{E_i}\right)^{\frac{1}{q}}}{T} f_{Ta_i}^q \tag{90}$$

$$\frac{\partial f_i^q}{\partial \mu} = Bq\frac{f_{E_i}}{T} f_{Ta_i}^{2q-1} \tag{91}$$

On substitution, we will get,

$$\left.\frac{\partial P}{\partial \mu}\right|_T = \frac{1}{V}\sum_i f_i^q = \frac{N}{V} \tag{92}$$

$$\left.\frac{\partial P}{\partial \mu}\right|_T = n' \tag{93}$$

2.5.4. Relation 4

Last equation which relates the derivative of pressure to the entropy density is given as

$$\left.\frac{\partial P}{\partial T}\right|_\mu = s \tag{94}$$

$$\frac{\partial P}{\partial T} = \frac{1}{V}\left[-\frac{\partial E}{\partial T} + S + T\frac{\partial S}{\partial T} + \mu\frac{\partial N}{\partial T}\right] \tag{95}$$

So to prove the above relation, we have to prove that basically

$$-\frac{\partial E}{\partial T} + T\frac{\partial S}{\partial T} + \mu\frac{\partial N}{\partial T} = 0 \tag{96}$$

Solving the equation above, we get

$$\begin{aligned} = \sum_i \Bigg[& -q f_i^{q-1} E_i \frac{\partial f_i}{\partial T} + \frac{Tq}{(q-1)(B f_E)^{\frac{1}{q}-1}} \frac{\partial f_i}{\partial T} \\ & - \frac{T q f_i^{q-1}}{q-1}\frac{\partial f_i}{\partial T} + \mu q f_i^{q-1}\frac{\partial f_i}{\partial T}\Bigg] \end{aligned} \tag{97}$$

On solving the above equation, we get zero which satisfies Equation (96). Hence,

$$\left.\frac{\partial P}{\partial T}\right|_\mu = s \tag{98}$$

This proves that the unified distribution along with the form of entropy given in Equation (57), is thermodynamically consistent. As shown above, the pass of the thermal test makes the unified distribution thermodynamically relevant equations for a generalization by fulfilling all required criteria.

As has been discussed earlier, the relevance of Tsallis distribution is only limited to the low-p_T region because of the dominance of hard processes in high-p_T. Unified distribution resolves this issue by generalizing the Tsallis distribution to include hard processes as well. In the next section, we have performed a comparative study of different distributions to prove that the unified distribution is indeed the best fit to explain transverse momentum spectra.

3. Results

To test the applicability of unified distribution, we have performed a detailed analysis of the invariant yield of π^+ over different energy ranges. The results shown below present the main body of validation obtained in this work, where, a comparison between BG, Tsallis, and unified statistical approaches in describing the transverse momentum spectra is demonstrated. It shows the degree of agreement between measured data and the results attainable by the approaches based on statistical thermodynamics. In the plots, symbols represent the experimentally measured data of transverse momentum, and solid lines represent the results fitted by BG, Tsallis, and unified distribution functions. The ROOT [47] data analysis framework has been used along with MINUIT [48] class for fitting.

The analysis was done for the transverse momentum data of π^+ particles produced in $Au - Au$ and $Pb - Pb$ collisions and the collision energies we selected for study included 19.6 GeV [49], 27 GeV [49], 39.0 GeV [49], 130 GeV [50], 200.0 GeV [51], and 2.76 TeV [52].

The goodness of the unified function approach over other approaches is determined by analyzing the *chi-square* values of each fit. We use the *chi-square* goodness of fit test to determine how the observed value is different from the expected value and to compare the observed sample distribution with the expected probability distribution. A table including the Chi-square values of Boltzmann, Tsallis, and unified functions fitted to p_T-spectra at several energies is given in Table 1.

Table 1. The χ^2/NDF values of transverse momentum data of π^+ particles fitted to Boltzmann, Tsallis, and unified functions at various collision energies.

$\sqrt{s_{NN}}$	χ^2/NDF		
	Boltzmann	**Tsallis**	**Unified**
19.6	9.769	0.392	0.052
27	9.934	0.316	0.040
39	10.299	0.275	0.003
130	45.747	5.118	1.912
200	337.676	14.567	1.798
2760	23.980	2.314	0.064

It is clearly evident from the fits in Figures 1–6 that the unified fits are better compared to Boltzmann and Tsallis fits. This can be confirmed from Table 1, where the χ^2/NDF values of all the fits are displayed. From Table 1, we observe that the χ^2/NDF values are minimum for unified fits at all the energies. As we expect, these are large for Boltzmann fits, and that of Tsallis fits are intermediate.

Boltzmann distribution is parameterized by only one parameter, which is the temperature (T). Tsallis framework includes another parameter called q-parameter apart from the temperature, which gives the extent of non-extensivity in the distribution. The proposed unified distribution approach comprises two more free parameters in addition to the temperature and q-parameter. The relation of unified function parameters with the higher-order moments could be a reason for its success over other distribution, most of which depends primarily on mean and standard deviation as parameters. Further, we observe that the Tsallis distribution deviates from data at the high-p_T region, which forms the tail part of the distribution. In addition, the tail part of a distribution is more sensitive to higher-order moments. This could be a statistical reason for the success of unified distribution, especially in high-p_T regime.

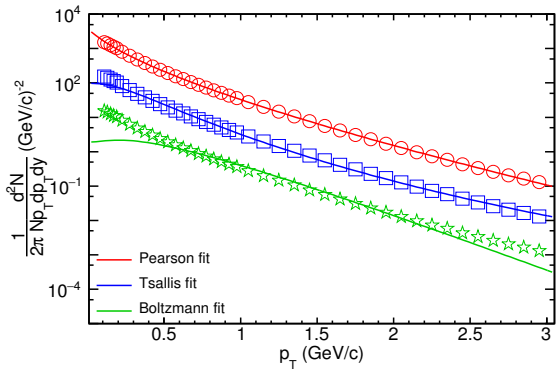

Figure 1. The transverse momentum spectra of π^+ particles produced in most central 2.76 TeV $Pb-Pb$ collision measured by the ALICE experiment [52] fitted with Boltzmann Equation (8), Tsallis Equation (16) and unified distribution function Equation (40). Data points are scaled for better visibility.

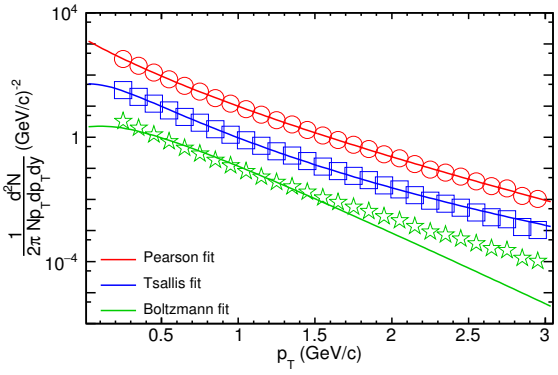

Figure 2. The transverse momentum data of π^+ particles produced in most central 200 GeV $Au - Au$ collision measured by the PHENIX experiment [51] fitted with Boltzmann Equation (8), Tsallis Equation (16) and unified distribution function Equation (40). Data points are scaled for better visibility.

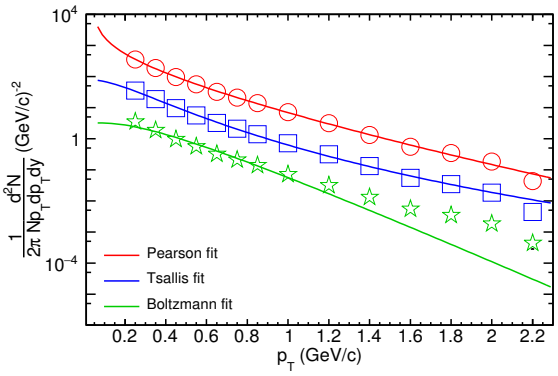

Figure 3. The transverse momentum data of π^+ particles produced in most central 130 GeV $Au - Au$ collision measured by the PHENIX experiment [50] fitted with Boltzmann Equation (8), Tsallis Equation (16) and unified distribution function Equation (40). Data points are scaled for better visibility.

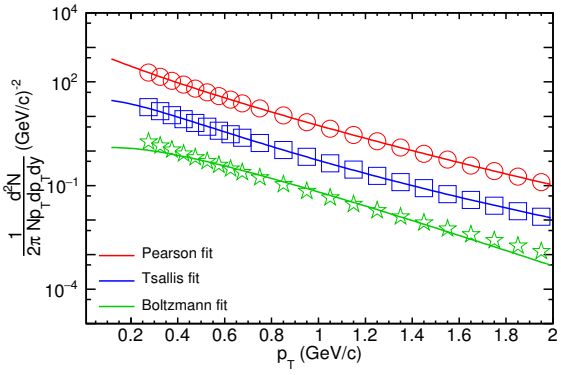

Figure 4. The transverse momentum data of π^+ particles produced in most central 39 GeV $Au - Au$ collision measured by the STAR experiment [49] fitted with Boltzmann Equation (8), Tsallis Equation (16) and unified distribution function Equation (40). Data points are scaled for better visibility.

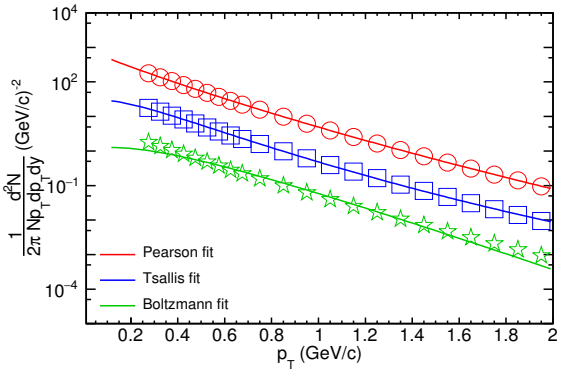

Figure 5. The transverse momentum data of π^+ particles produced in most central 27 GeV $Au-Au$ collision measured by the STAR experiment [49] fitted with Boltzmann Equation (8), Tsallis Equation (16) and unified distribution function Equation (40). Data points are scaled for better visibility.

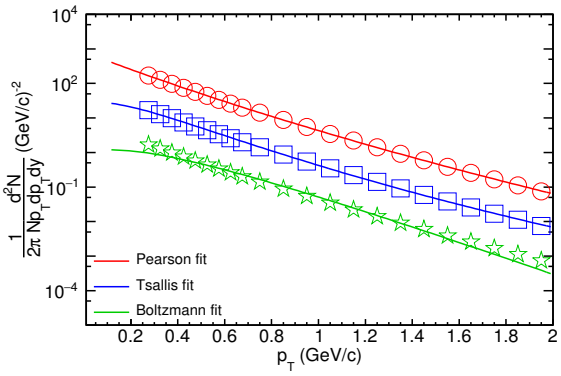

Figure 6. The transverse momentum data of π^+ particles produced in most central 19.6 GeV $Au-Au$ collision measured by the STAR experiment [49] fitted with Boltzmann Equation (8), Tsallis Equation (16) and unified distribution function Equation (40). Data points are scaled for better visibility.

The presence of a quenching effect beyond a certain p_T value in heavy-ion collision limits the application of the statistical thermal models; however, the absence of such an effect in pp collision makes it an ideal choice to test whether the developed formalism covers a broader range of p_T. Hence, to check the applicability of a unified statistical framework over a broad p_T range; we have considered the pp collision data, with p_T up to a few hundred GeV/c, and the yield spanning over several orders of magnitude. For this analysis, we have used the data of transverse momentum spectra of charged hadron produced in pp collision at four different energies ($\sqrt{s_{NN}} = 900$ GeV [53], 2.76 TeV [54], 5.02 TeV [55] and 7 TeV [53]) measured by CMS experiment over wide p_T range upto 400 GeV/c. Further, we have analyzed the recently released high multiplicity pp collision data at 7 TeV measured by ALICE experiment in different V0M event multiplicity classes [56] with the multiplicities corresponding to each class provided in Table 2. The pseudorapidity ranges of data at 0.9 TeV and 7 TeV is $|\eta| < 2.4$ [53], 2.76 TeV [54] and 5.02 TeV [55] is $|\eta| < 1$. At the same time, the corresponding range for the multiplicity class divided data measured by ALICE experiment at 7 TeV [56] is $|\eta| < 0.5$.

Figure 7 represents the unified function fit to p_T spectra for four different energies with p_T range up to 400 GeV. The corresponding fit to 7 TeV data divided into separate multiplicity classes is given in Figure 8. From the plot of the ratio of experimental data to the fit function, we observe a log-periodic oscillation over a broad range of transverse momenta for the unified statistical framework. This form of oscillation has been discussed for Tsallis distribution in Refs. [34,57,58]. Further, the oscillation observed in the 7 TeV

ALICE experiment data shows an interesting pattern over different multiplicity classes. Here we observe a clear reversal in the oscillation pattern as we go from the ALICE multiplicity class V0M 1 to V0M 10. This strange behavior in data overfit needs to be further explored, and it has the potential to give interesting physics information.

Table 2. VZERO multiplicity classes and the corresponding multiplicity values $\langle dN_{ch}/d\eta \rangle$.

Multiplicity Class	7 TeV pp Collision
V0M I	21.3 ± 0.6
V0M II	16.5 ± 0.5
V0M III	13.5 ± 0.4
V0M IV	11.5 ± 0.3
V0M V	10.1 ± 0.3
V0M VI	8.45 ± 0.25
V0M VII	6.72 ± 0.21
V0M VIII	5.4 ± 0.17
V0M IX	3.9 ± 0.14
V0M X	2.26 ± 0.12

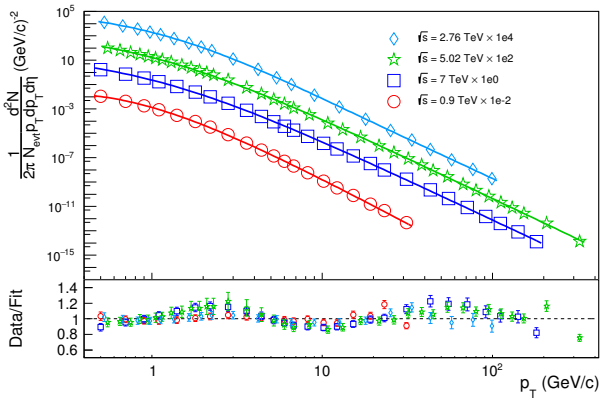

Figure 7. Top plot: The transverse momentum data of charged hadrons produced in pp collision at 0.9 TeV [53], 2.76 TeV [54], 5.02 TeV [55], and 7 TeV [53] measured by the CMS experiment fitted with unified distribution Equation (43). Bottom plot: Ratio of the experimental data to the corresponding value obtained from the fit function.

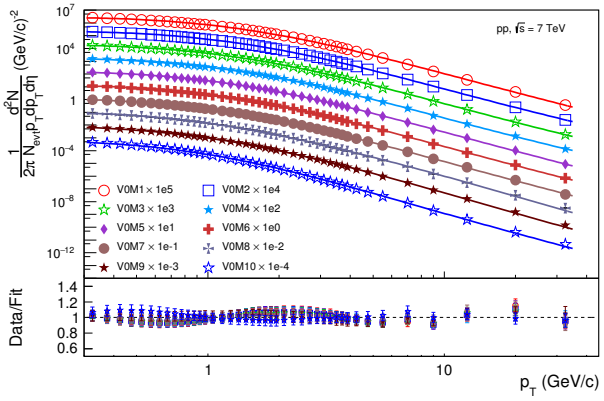

Figure 8. Top plot: The transverse momentum data of charged hadrons divided into multiplicity classes produced in pp collision at 7 TeV [56] measured by the ALICE experiment fitted with unified distribution Equation (43). Bottom plot: Ratio of the experimental data to the corresponding value obtained from the fit function.

In Table 3 and 4, we have provided the fitted value of temperature and q parameters that appear in the unified function Equation (43) and the χ^2/NDF values, which represent

the goodness of the fit. Low χ^2/NDF values in the tables suggest a good agreement between the experimental data and the unified distribution function. Ratio plots of different energies for unified function fit (Figures 7 and 8) also compliments the observation of goodness of fit to the experimental data.

Table 3. Best fit value of the parameters T (GeV) & q and the χ^2/NDF value obtained by fitting the charged hadron spectra produced in pp collision at 0.9 TeV [53], 2.76 TeV [54], 5.02 TeV [55], and 7 TeV [53] measured by the CMS experiment with the unified distribution function Equation (43).

Energy	T	q	χ^2/NDF
0.9 TeV	0.078 $\pm$0.009	1.032 $\pm$0.003	1.790
2.76 TeV	0.132 $\pm$0.006	1.070 $\pm$0.002	0.996
5.02 TeV	0.146 $\pm$0.007	1.122 $\pm$0.001	3.119
7 TeV	0.125 $\pm$0.001	1.147 $\pm$0.001	4.559

Table 4. Best fit value of the parameters T (GeV), q and the χ^2/NDF value obtained by fitting the multiplicity class divided charged hadron spectra produced in pp collision at 7 TeV measured by the ALICE experiment [56] with the unified distribution function Equation (43).

Mult. Class	T	q	χ^2/NDF
V0M I	0.221 $\pm$0.011	1.146 $\pm$0.004	0.996
V0M II	0.211 $\pm$0.010	1.145 $\pm$0.004	0.787
V0M III	0.202 $\pm$0.011	1.142 $\pm$0.005	0.639
V0M IV	0.194 $\pm$0.010	1.132 $\pm$0.005	0.518
V0M V	0.190 $\pm$0.017	1.136 $\pm$0.009	0.518
V0M VI	0.182 $\pm$0.017	1.129 $\pm$0.009	0.321
V0M VII	0.166 $\pm$0.003	1.114 $\pm$0.001	0.337
V0M VIII	0.167 $\pm$0.005	1.121 $\pm$0.002	0.107
V0M IX	0.156 $\pm$0.005	1.135 $\pm$0.003	0.377
V0M X	0.126 $\pm$0.005	1.077 $\pm$0.002	0.726

4. Discussion

The unified statistical framework is a more generalized approach to statistically explain the system created in ultra-high energy collisions. What distinguishes unified formalism from a simple polynomial fit is the richness of physics it incorporates. It is a thermodynamically consistent formalism following the laws of thermodynamics. The non-extensivity properties of the unified statistics evolved similarly to that of Tsallis statistics; however, one of the important distinctions between the two is the presence of additional parameters

p_0 and n in the former case whose connection with the physics observable needs to be explored to get the ultimate benefit of this formalism. One such effort has been made in Ref. [6], where the unified function parameter is shown to describe the second-order flow parameter v_2 nicely. A linear relationship has been established between the v_2 and the unified function parameter n using the charged hadron spectra produced in $Pb - Pb$ collision at 2.76 TeV.

The presence of more free parameters in unified formalism gives an extra advantage in terms of obtaining better-fit results as compared to Tsallis statistics. This can be verified from the result obtained in the previous section, where we observe an improvement in the quality of fit using unified formalism than the Tsallis statistics. This improvement can also be attributed to the unique approach where the physics of soft and hard processes are considered in a unified manner. We have also tested the applicability of unified formalism in small collision systems, and we have shown that the unified formalism provides a better fit to the pp collision data up to a few hundred GeV/c and over different energies and multiplicities.

One can also argue that a higher-order polynomial may do a better fitting; however, the richness of physics that unified formalism incorporates to make it a better choice being thermodynamically consistent. Moreover, unified formalism is backward compatible with Tsallis distribution under the limiting condition of the parameters. From the statistical perspective, the relation of unified distribution with higher-order moments such as skewness and kurtosis also makes it a suitable choice to fit a skewed dataset. This further strengthens the need for exploration of the unified statistical framework in other areas of high energy physics.

5. Conclusions

In this work, we have presented a comprehensive study of the theoretical framework to analyze transverse momentum spectra. Further, we have provided a detailed mathematical description of the unified distribution, which was first proposed in Ref. [6] and is proved to describe both soft and hard scattering regions of particle spectra in a unified manner. We have also demonstrated the applicability of unified distribution in the study of the p_{T}-spectra of different particles produced in a heavy-ion collision as well as the pp collision over a broad energy range. Further, we have also explored the thermodynamical consistency of unified distribution and proved that this distribution consistently follows the laws of thermodynamics.

This formalism has very wide applications in high-energy physics. We can utilize this formalism to extract several thermodynamic quantities such as the isothermal compressibility, speed of sound [59], chemical potential, and specific heat of the system created in the heavy-ion collision. This formalism can also be modified to study the pseudorapidity distribution [60] and the particle multiplicity.

In conclusion, we would like to point out that we have proposed a generalization to the Tsallis-like distribution function with a significant improvement in the goodness of fit to the spectra. We would also like to stress that although several theoretical and phenomenological works are proposed to study particle production in the high-energy collision, more novel ideas are required to tap into the full potential of the data obtained in mega collider experiments.

This paper provides a detailed theoretical description of the unified statistical framework and has the potential for wider applicability in other areas of physics.

Author Contributions: Conceptualization, S.J. (Satyajit Jena); Methodology, R.G.; Formal analysis, R.G., A.M. and S.J. (Shubhangi Jain); Data curation, S.J. (Shubhangi Jain); Writing—original draft, R.G.; Writing—review & editing, S.J. (Satyajit Jena); Supervision, S.J. (Satyajit Jena). All authors have read and agreed to the published version of the manuscript.

Funding: R. Gupta would like to acknowledge the financial support provided by CSIR through fellowship number 09/947 (0067) 2015-EMR-1.

Data Availability Statement: The data used for this analysis are already published and are cited at relevant places within the text as references.

Acknowledgments: A. Menon would like to acknowledge that this work was done during her association at IISER Mohali as a part of her thesis work.

Conflicts of Interest: The authors declare no conflict of interest.

References

1. Harrison, M.; Ludlam, T.; Ozaki, S. RHIC project overview. *Nucl. Instrum. Methods Phys. Res. A* **2003**, *499*, 235–244. [CrossRef]
2. Evans, L.; Bryant, P. LHC Machine. *JINST* **2008**, *3*, S08001. [CrossRef]
3. Jacobs, P.; Wang, X.N. Matter in extremis: Ultrarelativistic nuclear collisions at RHIC. *Prog. Part. Nucl. Phys.* **2005**, *54*, 443. [CrossRef]
4. Gyulassy, M.; Vitev, I.; Wang, X.N.; Zhang, B.W. Jet quenching and radiative energy loss in dense nuclear matter. *Quark Gluon Plasma* **2004**, *3*, 123–191. [CrossRef]
5. Kolb, P.F.; Heinz, U.W. Hydrodynamic description of ultrarelativistic heavy ion collisions. *Quark Gluon Plasma* **2003**, *3*, 634–714.
6. Jena, S.; Gupta, R. A unified formalism to study transverse momentum spectra in heavy-ion collision. *Phys. Lett. B* **2020**, *807*, 135551. [CrossRef]
7. Gupta, R.; Jena, S. Model Comparison of the Transverse Momentum Spectra of Charged Hadrons Produced in *PbPb* Collision at $\sqrt{s_{NN}}$ = 5.02 TeV. *Adv. High Energy Phys.* **2022**, *2022*, 5482034. [CrossRef]
8. Koppe, H.; Naturforschg, Z. Die Mesonenausbeute beim Beschuss von leichten Kernen mit Alpha-Teilchen. *Z. Naturforsch. A* **1948**, *3*, 251–252. [CrossRef]
9. Tawfik, A.N. Koppe's Work of 1948: A fundamental for non-equilibrium rate of particle production. *Z. Naturforsch. A* **2014**, *69*, 106. [CrossRef]
10. Fermi, E. High-energy nuclear events. *Prog. Theor. Phys.* **1950**, *5*, 570. [CrossRef]
11. Fermi, E. Angular Distribution of the Pions Produced in High Energy Nuclear Collisions. *Phys. Rev.* **1951**, *81*, 683. [CrossRef]
12. Hagedorn, R. Statistical thermodynamics of strong interactions at high-energies. *Nuovo Cim. Suppl.* **1965**, *3*, 147.
13. Hagedorn, R.; Ranft, J. Statistical thermodynamics of strong interactions at high-energies. 2. Momentum spectra of particles produced in pp-collisions. *Nuovo Cim. Suppl.* **1968**, *6*, 169.
14. Tawfik, A.N. Equilibrium statistical-thermal models in high-energy physics. *Int. J. Mod. Phys. A* **2014**, *29*, 1430021. [CrossRef]
15. Groot, S.R.D.; Leeuwen, W.A.V.; Weert, C.G.V. *Relativistic Kinetic Theory. Principles and Applications*; North-Holland: Amsterdam, The Netherlands, 1980; 417p.
16. Stodolsky, L. Temperature fluctuations in multiparticle production. *Phys. Rev. Lett.* **1995**, *75*, 1044–1045. [CrossRef]
17. Schnedermann, E.; Sollfrank, J.; Heinz, U.W. Thermal phenomenology of hadrons from 200-A/GeV S+S collisions. *Phys. Rev. C* **1993**, *48*, 2462-2475. [CrossRef] [PubMed]
18. Basu, S.; Chatterjee, R.; Nandi, B.K.; Nayak, T.K. Characterization of relativistic heavy-ion collisions at the Large Hadron Collider through temperature fluctuations. *arXiv* **2015**, arXiv:1504.04502.
19. Pulawski, S. Recent results from the strong interactions program of NA61/SHINE. *EPJ Web Conf.* **2017**, *164*, 07033. [CrossRef]
20. Tsallis, C. Possible Generalization of Boltzmann-Gibbs Statistics. *J. Statist. Phys.* **1988**, *52*, 479. [CrossRef]
21. Wilk, G.; Wlodarczyk, Z. On the interpretation of nonextensive parameter q in Tsallis statistics and Levy distributions. *Phys. Rev. Lett.* **2000**, *84*, 2770. [CrossRef]
22. Wilk, G.; Wlodarczyk, Z. Consequences of temperature fluctuations in observables measured in high energy collisions. *Eur. Phys. J. A* **2012**, *48*, 161. [CrossRef]
23. Cleymans, J.; Worku, D. Relativistic Thermodynamics: Transverse Momentum Distributions in High-Energy Physics. *Eur. Phys. J. A* **2012**, *48*, 160. [CrossRef]
24. Wilk, G.; Wlodarczyk, Z. The Imprints of nonextensive statistical mechanics in high-energy collisions. *Chaos Solitons Fractals* **2002**, *13*, 581. [CrossRef]
25. Tsallis, C. *Introduction to Nonextensive Statistical Mechanics*; Springer: New York, USA, 2009.
26. Gell-Mann, M.; Tsallis, C. *Nonextensive Entropy-Interdisciplinary Application*; Oxford University Press: New York, NY, USA, 2004.
27. Biro, T.S.; Molnar, E. Fluid dynamical equations and transport coefficients of relativistic gases with non-extensive statistics. *Phys. Rev. C* **2012**, *85*, 024905. [CrossRef]
28. Wilk, G.; Wlodarczyk, Z. Power laws in elementary and heavy-ion collisions: A Story of fluctuations and nonextensivity? *Eur. Phys. J. A* **2009**, *40*, 299. [CrossRef]
29. Biro, T.S.; Purcsel, G. Non-extensive Boltzmann equation and hadronization. *Phys. Rev. Lett.* **2005**, *95*, 162302. [CrossRef]
30. Si, R.F.; Li, H.L.; Liu, F.H. Comparing standard distribution and its Tsallis form of transverse momenta in high energy collisions. *Adv. High Energy Phys.* **2018**, *2018*, 7895967. [CrossRef]
31. De, B.; Bhattacharyya, S.; Sau, G.; Biswas, S.K. Non-extensive thermodynamics, heavy ion collisions and particle production at RHIC energies. *Int. J. Mod. Phys. E* **2007**, *16*, 1687. [CrossRef]
32. Arnison, G. et al. [UA1 Collaboration]. Transverse Momentum Spectra for Charged Particles at the CERN Proton anti-Proton Collider. *Phys. Lett.* **1982**, *118B*, 167. [CrossRef]

33. Tawfik, A.N. Out-Of-Equilibrium Transverse Momentum Spectra of Pions at LHC Energies. *Adv. High Energy Phys.* **2019**, *2019*, 4604608. [CrossRef]
34. Azmi, M.D.; Cleymans, J. The Tsallis Distribution at Large Transverse Momenta. *Eur. Phys. J. C* **2015**, *75*, 430. [CrossRef]
35. Cirto, L.J.L.; Tsallis, C.; Wong, C.Y.; Wilk, G. The transverse-momenta distributions in high-energy pp collisions—A statistical-mechanical approach. *arXiv* **2014**, arXiv:1409.3278.
36. Wong, C.Y.; Wilk, G. Tsallis fits to p_T spectra and multiple hard scattering in pp collisions at the LHC. *Phys. Rev. D* **2013**, *87*, 114007. [CrossRef]
37. Wong, C.Y.; Wilk, G.; Cirto, L.J.L.; Tsallis, C. Possible Implication of a Single Nonextensive p_T Distribution for Hadron Production in High-Energy pp Collisions. *EPJ Web Conf.* **2015**, *90*, 04002. [CrossRef]
38. Wong, C.Y.; Wilk, G. Tsallis Fits to p_{T} Spectra for pp Collisions at LHC. *Acta Phys. Polon. B* **2012**, *43*, 2047. [CrossRef]
39. Biyajima, M.; Mizoguchi, T.; Suzuki, N. Analyses of whole transverse momentum distributions in $p\bar{p}$ and pp collisions by using a modified version of Hagedorn's formula. *Int. J. Mod. Phys. A* **2017**, *32*, 1750057. [CrossRef]
40. Michael, C.; Vanryckeghem, L. Consequences of Momentum Conservation for Particle Production at Large Transverse Momentum. *J. Phys. G* **1977**, *3*, L151. [CrossRef]
41. Michael, C. Large Transverse Momentum and Large Mass Production in Hadronic Interactions. *Prog. Part. Nucl. Phys.* **1979**, *2*, 1. [CrossRef]
42. Hagedorn, R. Multiplicities, p_T Distributions and the Expected Hadron $\rightarrow$ Quark - Gluon Phase Transition. *Riv. Nuovo Cim.* **1983**, *6N10*, 1–50. [CrossRef]
43. Pearson, K. Contributions to the mathematical theory of evolution, II: Skew variation in homogeneous material *Philos. Trans. R. Soc. Lond. Math. Phys. Eng. Sci.* **1895**, *186*, 343.
44. Pollard, J.H. *A Handbook of Numerical and Statistical Techniques with Examples Mainly from the Life Sciences*; Cambridge University Press: Cambridge, UK, 1979.
45. Podladchikova, O.; Lefebvre, B.; Krasnoselskikh, V.; Podladchikov, V. Nonlinear Processes in Geophysics. *Eur. Geosci. Union (EGU)* **2003**, *10*, 323.
46. Behera, N.K. Constructing probability density function of net-proton multiplicity distributions using Pearson curve method. *arXiv* **2017**, arXiv:1706.06558.
47. Brun, R.; Rademakers, F. ROOT—An Object Oriented Data Analysis Framework. *Nucl. Instrum. Methods Phys. Res. Sec. A* **1997**, *A389*, 81–86. [CrossRef]
48. James, F.; Roos, M. Minuit: A System for Function Minimization and Analysis of the Parameter Errors and Correlations. *Comput. Phys. Commun.* **1975**, *10*, 343–367. [CrossRef]
49. Adamczyk, L. et al. [STAR Collaboration]. Bulk Properties of the Medium Produced in Relativistic Heavy-Ion Collisions from the Beam Energy Scan Program. *Phys. Rev. C* **2017**, *96*, 044904. [CrossRef]
50. Adcox, K. et al. [PHENIX Collaboration]. Centrality dependence of $pi^{+/-}$, $K^{+/-}$, p and $\overline{p}$ production from $\sqrt{s_{NN}}$ = 130 GeV Au+Au collisions at RHIC. *Phys. Rev. Lett.* **2002**, *88*, 242301. [CrossRef]
51. Adler, S.S. et al. [PHENIX Collaboration]. Identified charged particle spectra and yields in Au+Au collisions at $\sqrt{s_{NN}}$ = 200 GeV. *Phys. Rev. C* **2004**, *69*, 034909. [CrossRef]
52. Abelev, B. et al. [ALICE Collaboration]. Centrality dependence of π, K, p production in Pb-Pb collisions at $\sqrt{s_{NN}}$ = 2.76 TeV. *Phys. Rev. C* **2013**, *88*, 044910. [CrossRef]
53. Chatrchyan, S. et al. [CMS Collaboration]. Charged particle transverse momentum spectra in pp collisions at $\sqrt{s}$ = 0.9 and 7 TeV. *JHEP* **2011**, *8*, 86. [CrossRef]
54. Chatrchyan, S. et al. [CMS Collaboration]. Study of high-pT charged particle suppression in PbPb compared to pp collisions at $\sqrt{s_{NN}}$ = 2.76 TeV. *Eur. Phys. J. C* **2012**, *72*, 1945. [CrossRef]
55. Khachatryan, V. et al. [CMS Collaboration]. Charged-particle nuclear modification factors in PbPb and pPb collisions at $\sqrt{s_{\mathrm{N\,N}}}$ = 5.02 TeV. *JHEP* **2017**, *4*, 39. [CrossRef]
56. Acharya, S. et al. [ALICE Collaboration]. Multiplicity dependence of light-flavor hadron production in pp collisions at $\sqrt{s}$ = 7 TeV. *Phys. Rev. C* **2019**, *99*, 024906. [CrossRef]
57. Wilk, G.; Wlodarczyk, Z. Log-periodic oscillations of transverse momentum distributions. *arXiv* **2014**, arXiv:1403.3508.
58. Wilk, G.; Włodarczyk, Z. Tsallis distribution with complex nonextensivity parameter q. *Phys. A* **2014**, *413*, 53–58. [CrossRef]
59. Jain, S.; Gupta, R.; Jena, S. Study of isothermal compressibility and speed of sound in matter formed in heavy-ion collision using unified formalism. *arXiv* **2021**, arXiv:2103.15117.
60. Gupta, R.; Katariya, A.S.; Jena, S. A unified formalism to study the pseudorapidity spectra in heavy-ion collision. *Eur. Phys. J. A* **2021**, *57*, 224. [CrossRef]